





Pressure-dependent dielectric response of the frustrated Mott insulator κ -(BEDT-TTF)₂Ag₂(CN)₃

R. Rösslhuber , R. Hübner , and M. Dressel ^{*}

1. Physikalisches Institut, Universität Stuttgart, Pfaffenwaldring 57, 70569 Stuttgart Germany

A. Pustogow [†]

Institute of Solid State Physics, TU Wien, 1040 Vienna, Austria



(Received 2 December 2022; accepted 23 January 2023; published 7 February 2023)

We explore the dielectric properties of the molecular quantum-spin-liquid candidate κ -(BEDT-TTF)₂Ag₂(CN)₃ as a function of frequency, pressure, and temperature. The transition from the incoherent semiconducting to the Mott-insulating state at the quantum Widom line yields a drop of the low-frequency dielectric constant to small positive values $\epsilon_1 \approx 10$. The characteristic relaxor-type peak around $T = 50$ K moves to lower temperatures when pressurized. An additional feature appears and quickly grows as the percolative first-order transition is approached with rising pressure. Above 4 kbar, it dominates the dielectric response and rapidly shifts to $T \rightarrow 0$. Overall, the pressure-dependent dielectric response is remarkably similar to the less-correlated sister compound κ -(BEDT-TTF)₂Cu₂(CN)₃. At the Mott transition, we identify a reentrant insulating behavior at $T^* = 11$ K which might indicate a low-entropy ground state — possibly with a spin gap.

DOI: [10.1103/PhysRevB.107.075113](https://doi.org/10.1103/PhysRevB.107.075113)

I. INTRODUCTION

The Mott transition has been intensely studied over the last decades in cuprates and other transition-metal compounds, as well as organic conductors, which — together with vanadium oxides — became the prime example for bandwidth-tuned insulator-metal transitions (IMTs) [1–4]. Recently, special focus was put on geometrically frustrated materials in the quest for quantum spin liquids (QSLs) [5–8]. This way, pressure-dependent studies have unveiled the physics of the genuine Mott state in the absence of antiferromagnetic order [9], in quantitative agreement with theoretical predictions of the single-band Hubbard model [10,11].

The dielectric properties of triangular-lattice molecular compounds κ -(BEDT-TTF)₂Cu₂(CN)₃, κ -(BEDT-TTF)₂Ag₂(CN)₃ and EtMe₃Sb[Pd(dmit)₂]₂ without magnetic order yield a relaxor-ferroelectric peak that has been controversially discussed over the past decade [12–16]. By simple and compelling arguments, Fukuyama *et al.* pointed out that the small intensity and low frequency of the dielectric anomaly ($\hbar\omega/U \approx 10^{-11}$ – 10^{-8} , where the typical frequencies are $\omega/2\pi = f = 10^3$ – 10^6 Hz and the Coulomb repulsion $U \approx 0.3$ eV [9]) suggest an origin related to disorder and inhomogeneities on larger length scales [17]. By applying pressure, we could elucidate this issue in κ -(BEDT-TTF)₂Cu₂(CN)₃ [18–20]: The correlation-driven metal-insulator transition is of first order; phase coexistence is therefore inherent. In other words, percolative effects are expected to inevitably accompany the Mott transition when temperature or pressure are varied.

While pressure-dependent dc measurements of the electrical resistivity were reported early on [21–24] for most organic Mott compounds, dielectric studies through the IMT are limited to κ -(BEDT-TTF)₂Cu₂(CN)₃ so far. To that end, it is highly desirable to extend such endeavors also to other frustrated Mott insulators.

Here, we carried out pressure-dependent dielectric experiments on κ -(BEDT-TTF)₂Ag₂(CN)₃ single crystals, yielding remarkably similar results and conclusions to the sister compound κ -(BEDT-TTF)₂Cu₂(CN)₃. As pressure increases, the well-known relaxor-ferroelectric response gets overwhelmed by a rapidly growing dielectric feature at lower temperatures, which is attributed to the percolative nature of the Mott transition. Several interesting details observed provide a fresh view on the dielectric response and the correlation-driven Mott transition in the title compound.

II. STATE OF THE ART

Figure 1(a) illustrates the schematic phase diagram of frustrated Mott insulators in the absence of magnetic order and spin-gapped states [18,26,27]. At elevated temperatures, thermally activated processes dominate the semiconducting behavior in a broad range. Depending on the strength of the effective correlations, the behavior becomes distinct at low temperatures (LTs): For strong electron-electron interactions, a crossover to the Mott-insulating regime occurs at the quantum Widom line (QWL). When the correlation effects are weaker – for instance, by applying pressure, the system turns metallic below the Brinkman-Rice temperature T_{BR} and eventually enters a Fermi-liquid (FL) phase. While the Mott state and its IMT are commonly discussed in terms of electrical conductivity, the dielectric properties provide an alternative and rather illuminating aspect. The permittivity ϵ_1 acquires

^{*}dressel@pi1.physik.uni-stuttgart.de

[†]pustogow@ifp.tuwien.ac.at

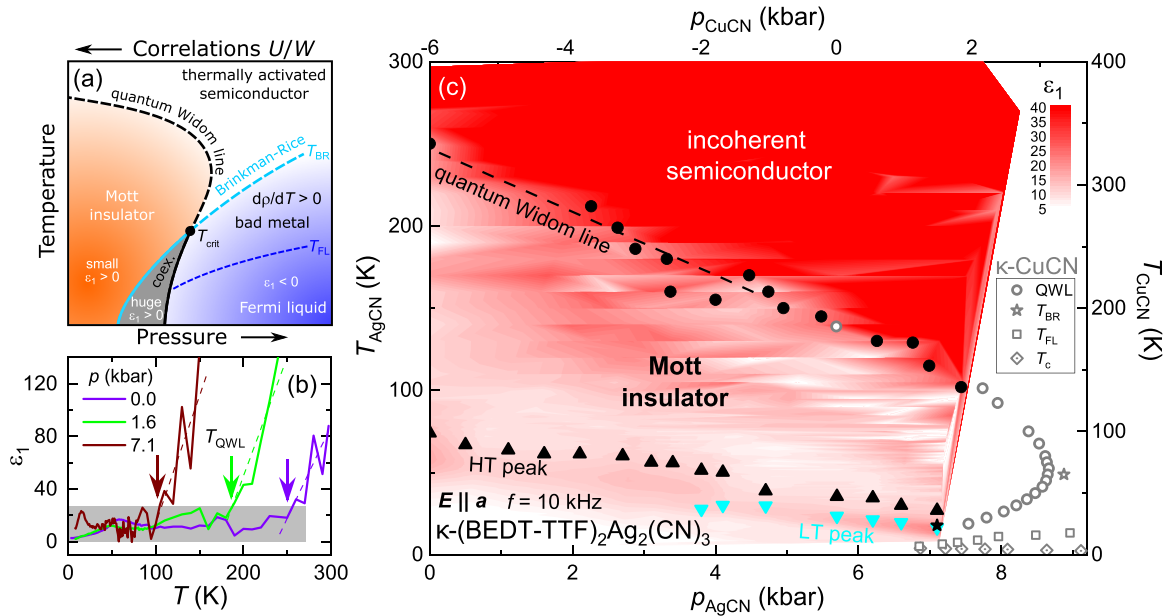


FIG. 1. (a) In general, the bandwidth-tuned Mott transition at half filling yields pronounced changes in the low-frequency dielectric constant ϵ_1 . The opening of a spectral gap at the quantum Widom line (QWL) results in a small, positive permittivity $\epsilon_1 \approx 10$ in the Mott-insulating state. In the close vicinity of the insulator-metal transition, a percolating regime with colossal values $\epsilon_1 \gg 10^2$ emerges due to the first-order coexistence regime, followed by negative permittivity in the metallic phase [18–20]. (b) In the case of κ -(BEDT-TTF) $_2$ Ag $_2$ (CN) $_3$, the rapid increase of ϵ_1 indicates the closing of the Mott gap ($\epsilon_1 \propto \Delta^{-2}$) at the crossover from the Mott insulator to a thermally activated semiconducting regime; consistent with transport results [9]. (c) A false color plot of the pressure-dependent data obtained on κ -(BEDT-TTF) $_2$ Ag $_2$ (CN) $_3$ at $f = 10$ kHz illustrates the Mott phase with $\epsilon_1 \approx 10$ (light red). The QWL lines up with the less correlated sister compound κ -(BEDT-TTF) $_2$ Cu $_2$ (CN) $_3$. Note, the pressure and temperature scales are shifted according to U/W scaling derived in Ref. [9]; the agreement is excellent. The solid black dots are the present results of the QWL determined from the 10 kHz data in panel (b), whereas the black and cyan triangles indicate the HT and LT peaks obtained from our dielectric data at 100 kHz (cf. Figs. 3 and 4). The open grey symbols indicate the QWL results (circles, from Refs. [9,25]), the onset of metallic behavior (star, Brinkman-Rice temperature T_{BR}), the Fermi-liquid temperature T_{FL} (square), and the superconducting transition temperature T_c (diamond) of κ -(BEDT-TTF) $_2$ Cu $_2$ (CN) $_3$ [26].

small, positive values of order 10 in the Mott-insulating state, reflecting the charge-excitation gap $\epsilon_1 \propto \Delta^{-2}$ in the quasistatic limit, i.e., for frequencies $f \ll \Delta$, the Mott gap. This way, the dielectric constant is enhanced while approaching the IMT [28], but this mechanism does not result in a true divergence due to the first-order character of the transition. Instead, a colossal enhancement of $\epsilon_1 \approx 10^3 - 10^5$ occurs in the coexistence regime of percolating metallic clusters embedded in an insulating matrix [18–20]. On the metallic side, the permittivity exhibits large negative values due to screening, consistent with ϵ_1 determined from optical spectroscopy [20,26].

For our investigations, we synthesized high-quality κ -(BEDT-TTF) $_2$ Ag $_2$ (CN) $_3$ single crystals by standard electrochemical methods [23,29]. Broadband dielectric spectroscopy was carried out in a pseudo-four-point configuration (out of plane, $E \perp bc$) as a function of pressure, temperature, and frequency using an Agilent 4294 impedance analyzer. The pressure-dependent investigations were performed utilizing a piston-type pressure cell up to approximately 10 kbar. Daphne oil 7373 serves as the liquid pressure-transmitting medium. For *in situ* determination of the actual pressure, an InSb semiconductor pressure gauge was incorporated in the cell. Unless indicated otherwise, throughout the paper we state the pressure reading at the lowest temperature, $T = 10$ K. A custom-made continuous-flow helium cryostat reduces the total cable length to 50 cm, enabling reliable

measurements at frequencies up to 5 MHz; the tradeoff is the low-temperature limit of 8 K. Further details are presented in Refs. [19,30].

In line with the above description, our dielectric experiments on κ -(BEDT-TTF) $_2$ Ag $_2$ (CN) $_3$ covering the insulating regime up to the IMT show small $\epsilon_1 \approx 10$ in the Mott state, which is presented in Figs. 1(b) and 1(c). The permittivity exhibits a pronounced enhancement above the QWL due to the closing of the Mott gap as incoherent semiconducting behavior sets in at higher temperatures. We extract the QWL from temperature-dependent dielectric measurements $\epsilon_1(T)$ as indicated in Fig. 1(b) for all pressures and, this way, obtain a precise mapping of the crossover temperature in the contour plot in Fig. 1(c). Our results are in excellent agreement with the universal QWL obtained from dc transport data of several QSL candidates, such as the title compound, EtMe $_3$ Sb[Pd(dmit) $_2$] $_2$ and κ -(BEDT-TTF) $_2$ Cu $_2$ (CN) $_3$ [23,25], when quantitatively scaled by the respective bandwidth [9]. Due to experimental limitations, the present investigations are confined to the insulating state, approaching the IMT boundary, but crossing it only slightly. Dielectric data under pressure could be acquired up to 7.1 kbar and down to 8 K, which precludes detailed studies of metallic and superconducting behavior, that is reported at lower temperatures ($T_c = 5.2$ K) and higher pressures ($p_c > 10$ kbar) [23]. The close vicinity to the phase coexistence regime is evident from the occurrence of $d\rho/dT > 0$ below $T_{BR} = 18$ K at 7.1 kbar.

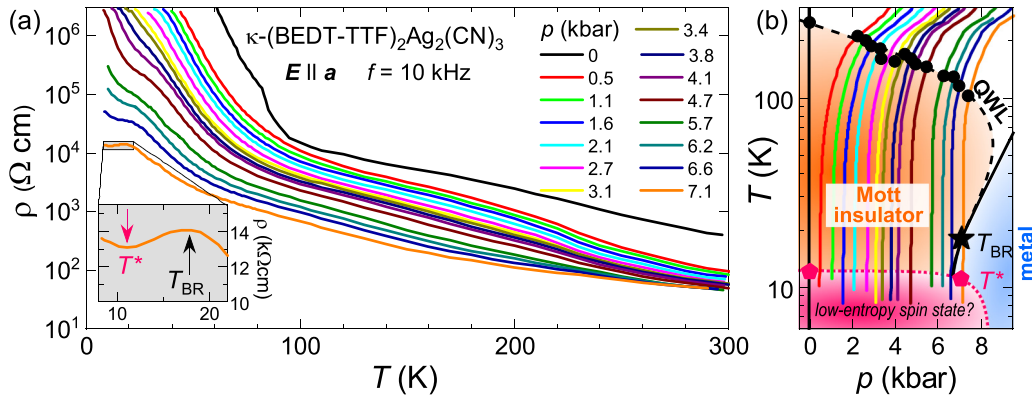


FIG. 2. (a) Pressure evolution of the temperature-dependent electrical resistivity $\rho(T)$ of κ -(BEDT-TTF) $_2$ Ag $_2$ (CN) $_3$ measured along a direction at $f = 10$ kHz. Upon increasing pressure, ρ continuously decreases while the overall insulating behavior with $d\rho/dT < 0$ is maintained. Due to the pressure loss upon cooling and limitations of our setup towards high pressures ($p \leq 10$ kbar at 300 K) and low temperatures ($T \geq 8$ K) [19], we barely reached the insulator-metal transition at 7.1 kbar. We expect superconductivity and Fermi-liquid behavior at lower temperatures and higher pressures. Apart from the resistivity maximum at $T_{BR} = 18$ K associated with the onset of metallic transport, the inset reveals a reentrance of insulating behavior at $T^* = 11$ K, reminiscent of the reentrance to the spin-gapped state in κ -(BEDT-TTF) $_2$ Cu $_2$ (CN) $_3$ [31]. (b) We included T^* from (a) and the extremum of the ambient-pressure thermal expansion coefficient α_a at 12 K from Ref. [32] in the phase diagram at $p = 0$ —possibly a sign of a low-entropy spin state at low temperatures. We also added the QWL and T_{BR} from Fig. 1(c). Solid lines indicate the trajectories of our experimental data, determined by *in situ* pressure measurements. The legend in panel (a) indicates the low-temperature pressure p at $T = 10$ K.

III. RESULTS

Figure 2 displays the resistivity curves for κ -(BEDT-TTF) $_2$ Ag $_2$ (CN) $_3$ at various pressures as indicated; the data are recorded at $f = 10$ kHz. Upon increasing pressure, $\rho(T)$ continuously decreases while the overall insulating behavior with $d\rho/dT < 0$ is maintained for all measurements. Figure 2(b) documents the *in situ* measured pressure: Upon cooling, a significant pressure loss occurs. Since our setup is restricted to a starting pressure of 10 kbar at room temperature, that is reduced upon cooling, we were barely able to reach the IMT. At the highest pressure of $p = 7.1$ kbar (determined *in situ* at $T = 10$ K), the resistivity exhibits a maximum around $T_{BR} = 18$ K as highlighted in the bottom left inset of Fig. 2(a). Notably, at this pressure we can also identify a reentrance of insulating behavior below $T = 11$ K, which reminds us of the reentrant insulating behavior in κ -(BEDT-TTF) $_2$ Cu $_2$ (CN) $_3$, where the low-entropy spin-gapped phase stabilizes below the metal [31]. We note that for κ -(BEDT-TTF) $_2$ Ag $_2$ (CN) $_3$, the temperature of the resistance minimum lines up with an anomaly of the thermal-expansion coefficient around 12 K [32]. Altogether, our data suggest the transition to a low-entropy state at $T^* = 11$ K, which deserves dedicated investigation in future work.

The signatures of $\rho(T, p)$ line up well with the dc-transport results by Shimizu *et al.* [23] and serve as a good reference for classifying the observed dielectric response as a function of pressure and temperature. Figure 3 presents the pressure evolution of the dielectric response of κ -(BEDT-TTF) $_2$ Ag $_2$ (CN) $_3$ by plotting $\epsilon_1(T)$ for different frequencies and pressures as indicated. At ambient pressure and below $T = 100$ K, we observe a broad peak in $\epsilon_1(T)$ which shifts to higher temperatures and decreases in amplitude for increasing frequencies [Fig. 3(a)]. These findings are in full

agreement with previous ambient-pressure reports by Pinterić *et al.* [15,16]. The peak features the same signature as the relaxor-ferroelectric response observed in the sibling compound κ -(BEDT-TTF) $_2$ Cu $_2$ (CN) $_3$ [12,14,16], with the difference that for κ -(BEDT-TTF) $_2$ Ag $_2$ (CN) $_3$ it occurs at higher temperatures ($T \approx 50$ K) and develops a larger amplitude. It is straightforward to label this relaxor ferroelectric peak the HT (high temperature) peak in analogy to the nomenclature we introduced for the Cu analog [19]. A closer look reveals an additional shoulderlike feature below 50 K which is more pronounced for higher frequencies. As we will see in the following, this shoulder does not correspond to the LT peak but constitutes an additional, distinct feature, that we refer to as anomaly (A) from now on.

When discussing how the feature varies with pressure, we can confine ourselves to the low-frequency response, where the peak is most pronounced. From ambient pressure up to $p = 2.1$ kbar [Figs. 3(a)–3(e)], the HT peak shifts to lower temperatures and slightly loses amplitude, while the A feature keeps its shoulderlike shape and does not change noticeably as a function of pressure. As pressure rises [Figs. 3(f)–3(j)], the HT maximum diminishes further while A strengthens and eventually becomes a well-defined peak which, for instance, is located around 13 K at $p = 4.1$ kbar. Starting from 2.7 kbar, a third feature appears in between the HT peak and the anomaly, located around 30 K and eventually dominating $\epsilon_1(T)$ at 4.7 kbar [Fig. 3(k)]. Upon increasing the pressure further up to 7.1 kbar [Figs. 3(k)–3(o)], the HT peak continues to move to lower temperatures as pressure rises while keeping its magnitude. Simultaneously, the third feature strongly grows in amplitude and shifts toward lower temperatures, masking the anomaly previously observed around 13 K. There is a striking agreement between the pressure evolution of the third feature and the one observed for the LT peak in

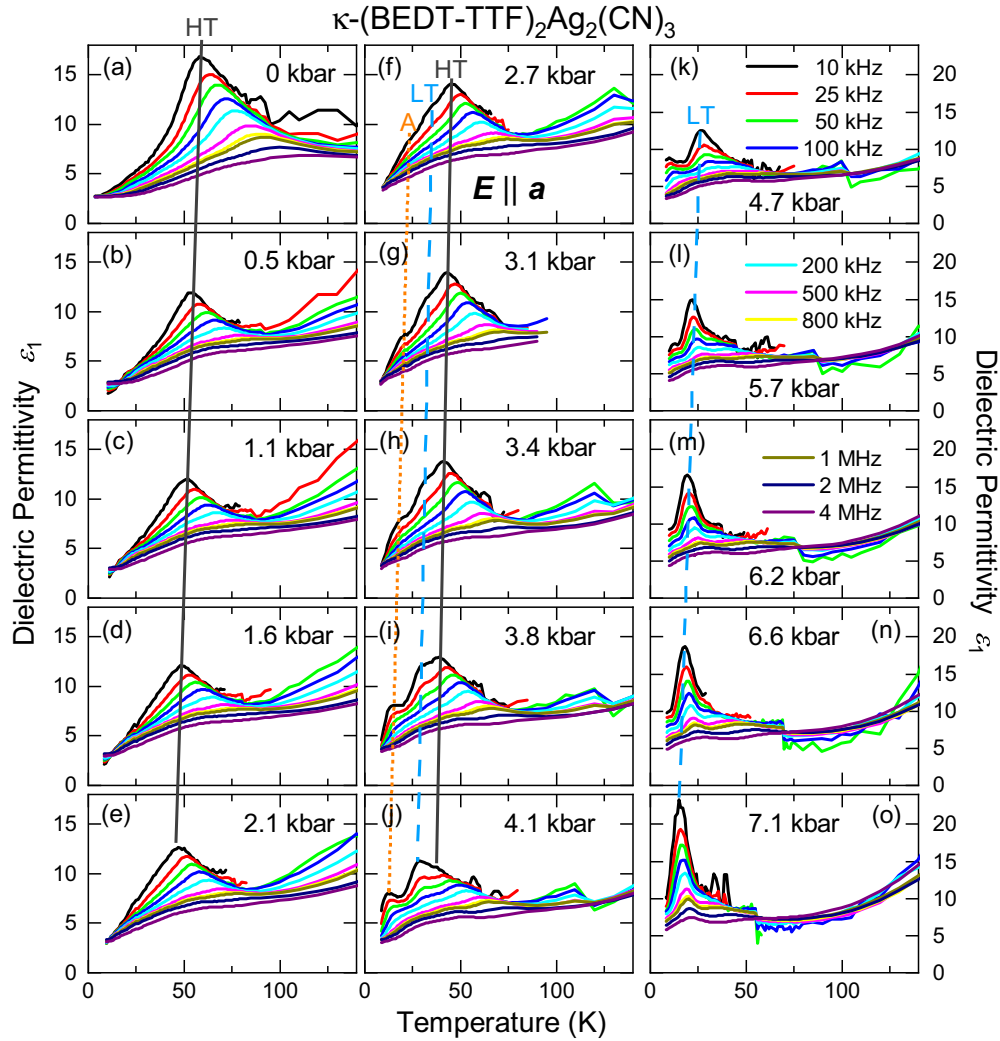


FIG. 3. Dielectric permittivity $\epsilon_1(T)$ of κ -(BEDT-TTF) $_2$ Ag $_2$ (CN) $_3$ as a function of temperature measured at several frequencies for different pressure values. (a) At 0 kbar and below 100 K, a broad dispersive peak dominates $\epsilon_1(T)$ reminiscent of relaxor ferroelectricity [12,15] which is labeled the HT peak [19]; the solid black line is a guide to the eye. Additionally, a shoulderlike anomaly (A) is revealed below 50 K. (b)–(g) Upon increasing pressure, the HT peak shifts toward lower temperatures and slightly diminishes in amplitude while the anomaly feature remains unchanged. (h)–(j) Upon increasing the pressure from 3.4 kbar to 4.7 kbar, the HT peak continues to shift toward lower temperatures and A develops into a well-defined peak (orange dotted line) which, for instance, is located around 13 K at 4.1 kbar. Simultaneously, a third feature becomes apparent in between the HT peak and the anomaly, eventually dominating $\epsilon_1(T)$ at 4.7 kbar, which we refer to as the LT peak (blue dashed line). (k)–(o) Upon further pressurizing the sample up to 7.1 kbar, the LT peak grows in amplitude and shifts toward lower temperatures, overwhelming the feature A and the HT peak. Note the different vertical scales between (a)–(j) and (k)–(o). The pressure values refer to the low-temperature pressure.

κ -(BEDT-TTF) $_2$ Cu $_2$ (CN) $_3$ [19], clearly identifying it as the LT peak in κ -(BEDT-TTF) $_2$ Ag $_2$ (CN) $_3$.

At this point, we can conclude far-reaching analogies between the sibling compounds as far as the HT and LT peaks are concerned in $\epsilon_1(T)$. The A anomaly in κ -(BEDT-TTF) $_2$ Ag $_2$ (CN) $_3$ is an additional feature that deserves further scrutiny. In the following, we give a detailed analysis and discussion of the pressure and frequency evolution of these dielectric features.

IV. ANALYSIS

To deconvolve peaks in the temperature-dependent dielectric constant and to trace their pressure variation, in particular,

we fit $\epsilon_1(T)$ at 100 kHz with two Gaussian modes accounting for the HT and the anomaly (A) peak. For $p > 3.4$ kbar, we introduce an additional Gaussian to model the LT peak. The resulting fits, together with their contributions, are plotted in Fig. 4(a) for selected pressures. The obtained fit parameters are displayed as a function of pressure in Figs. 4(b)–4(d). The HT peak position T_{HT} continuously shifts to lower temperatures with a slight bump around 3 kbar [Fig. 4(b)]. The latter is also observed for T_A , where it is even more pronounced. Most likely, the bump in T_{HT} and T_A is a precursor of the LT peak. The width appears rather volatile, especially for the anomaly at low pressures where it is not that strongly pronounced yet. The area of the Gaussian is a direct measure for the contribution of corresponding peak to $\epsilon_1(T)$ [Fig. 4(d)].

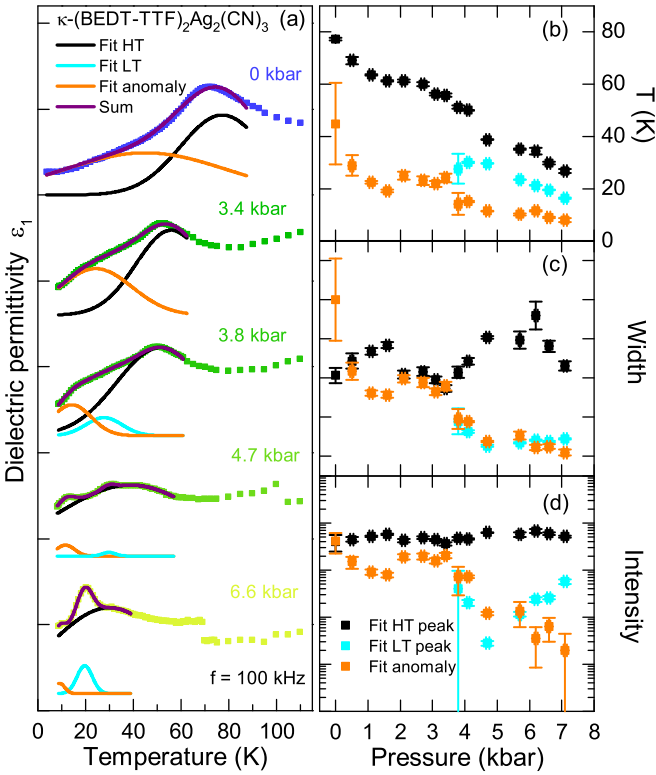


FIG. 4. (a) Fits of the HT and anomaly peak in $\epsilon_1(T)$ of κ -(BEDT-TTF) $_2$ Ag $_2$ (CN) $_3$ with two Gaussians for low-pressure data; to describe the LT mode at higher pressure ($p \geq 3.4$ kbar) a third Gaussian mode is introduced. (b) Pressure dependence of peak maxima, (c) the Gaussian peak width and (d) the intensity, given by integrated peak area.

It stays constant for the HT peak from ambient pressure up to 7.1 kbar. It exhibits a maximum around 3 kbar for the anomaly, which again is most likely due to the emerging LT peak, which is not accounted for separately yet. The area of the LT peak grows upon increasing the pressure from 4.7 to 7.1 kbar, clearly rising above the one of the anomaly peak. While the LT intensity is smaller than that of the HT peak at 100 kHz (Fig. 4), it becomes the dominant contribution at $f = 10$ kHz [Figs. 3(k)–3(o)] for high pressures due to its stronger enhancement with lower frequencies.

A. Pressure evolution of mode 1

To obtain a better physical insight, we fit the frequency dependence of the complex permittivity $\hat{\epsilon}(\omega) = \epsilon_1(\omega) + i\epsilon_2(\omega)$ of κ -(BEDT-TTF) $_2$ Ag $_2$ (CN) $_3$ taken at fixed temperature and pressure with two Cole-Cole modes according to

$$\hat{\epsilon}(\omega) - \epsilon_{\text{inf}} = \frac{\Delta\epsilon_1}{1 + (i\omega\tau_1)^{1-\alpha_1}} + \frac{\Delta\epsilon_2}{1 + (i\omega\tau_2)^{1-\alpha_2}}, \quad (1)$$

wherein $\tau_{1,2}$ are the relaxation times, $f = \omega/2\pi$ the frequency of the applied electric ac field, $(1 - \alpha_{1,2})$ are the parameters describing the symmetric broadening of the relaxation-time distribution functions, $\Delta\epsilon_{1,2}$ are the dielectric strengths of the corresponding modes, with $\Delta\epsilon_1 + \Delta\epsilon_2 = \epsilon_{\text{static}} - \epsilon_{\text{inf}}$, wherein ϵ_{static} and ϵ_{inf} are the values for low and high frequencies, respectively. The obtained fit parameters for mode

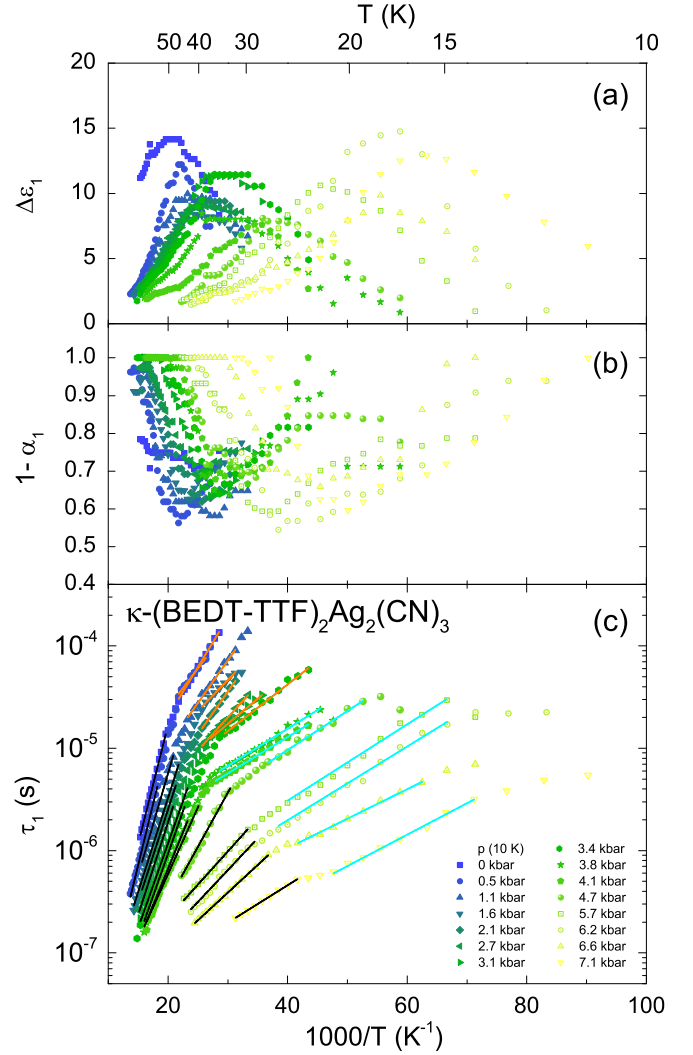


FIG. 5. Cole-Cole parameters of mode 1 plotted as a function of inverse temperature $1/T$ for different pressure values as indicated. (a) Dielectric strength $\Delta\epsilon_1(T)$, (b) distribution of relaxation times $1 - \alpha_1(T)$, and (c) mean relaxation time $\tau_1(T)$ of κ -(BEDT-TTF) $_2$ Ag $_2$ (CN) $_3$. The black lines represent fits with Eq. (2) above the kink in $\tau_1(T)$ at T_B . For $T < T_B$, fits of $\tau_1(T)$ with Eq. (2) are indicated by orange and cyan lines which are assigned to the anomaly and LT peak, respectively.

1 are plotted in Fig. 5 as a function of inverse temperature. We observe a pronounced peak in $\Delta\epsilon_1(T)$ shifting to lower temperatures as pressure is applied, reminiscent of the pressure evolution of $\epsilon_1(T)$ (Fig. 3). Interestingly, the amplitude of the peak first diminishes upon pressurizing and starts to rise again for $p \geq 4.7$ kbar (green spheres) right where the LT peak in $\epsilon_1(T)$ starts growing. The broadening parameter $(1 - \alpha_1)$ shows a pronounced minimum which is rather shallow from 0 to 3.1 kbar and gets strongly pronounced and broader above 3.4 kbar [Fig. 5(b)]. The application of pressure moves the position of the minimum toward lower temperatures, coinciding with the peak position in $\Delta\epsilon_1(T)$. The relaxation time $\tau_1(T)$ slows down upon cooling. In Fig. 5(c), we see a clear kink, which shifts to lower temperatures as pressure increases, while the corresponding relaxation time

gets shorter. In analogy to the nomenclature introduced for κ -(BEDT-TTF)₂Cu₂(CN)₃ [19], we denote the kink position as the bifurcation temperature T_B .

It is important to mention that upon increasing the pressure from 3.4 to 3.8 kbar, a considerable drop in $\tau_1(T)$ for $T < T_B$ is observed, which coincides with the appearance of the LT peak in $\varepsilon_1(T)$. Therefore, it is reasonable to attribute the relaxation dynamics observed in $\tau_1(T)$ for $p < 3.4$ kbar to the anomaly and for $p > 3.4$ kbar to the LT peak. This assignment will be confirmed below in Sec. IV C.

For all pressures investigated, $\tau_1(T)$ above and below T_B can be well described by an activated behavior:

$$\tau_1 = \tau_i \exp \left\{ \frac{\Delta_i}{T} \right\}. \quad (2)$$

Following the arguments above, the black, orange, and cyan lines in the Arrhenius plot Fig. 5(c) indicate the fits attributed to the respective peaks ($i = \text{HT, A, and LT}$). The intersection of fits precisely determines T_B , as we will show in detail later (Fig. 8).

Figures 6(a) and 6(b) presents the parameters obtained from fitting $\tau_1(T)$ with Eq. (2). The activation energy Δ_{HT} of the HT peak decreases with rising pressure, exhibiting a small bump around 3 kbar. Up to 2 kbar, the activation energy of the anomaly peak stays constant with $\Delta_A \approx 180$ K and then slightly drops to 100 K when pressure rises to $p = 3.4$ kbar. For pressures exceeding 3.4 kbar, the anomaly peak is masked by the growing LT peak such that the relaxation dynamics observed for $T < T_B$ are governed by the latter; its activation energy remains constant around $\Delta_{\text{LT}} \approx 80$ K up to 7.1 kbar. From ambient pressure up to 3.4 kbar, τ_A is fluctuating between 10^{-7} and 10^{-6} s. In the same pressure range, τ_{HT} is constant around 5×10^{-10} s and then significantly slows down for pressure exceeding 3.4 kbar. Starting from 3.8 kbar up to 7.1 kbar, τ_{LT} decreases by two orders of magnitude reminiscent to the behavior of the corresponding parameter in κ -(BEDT-TTF)₂Cu₂(CN)₃. In Fig. 6(c), we additionally plot the peak positions T_{HT} , T_A , and T_{LT} together with T_B to emphasize the assignment of the relaxation dynamics to the corresponding peak observed in $\varepsilon_1(T)$ (cf. Fig. 4). The pressure evolutions of Δ_{HT} and Δ_A resemble the ones of T_{HT} and T_A , respectively. In contrast to that, Δ_{LT} stays constant while T_{LT} decreases to 16.5 K upon pressurizing up to 7.1 kbar.

B. Pressure evolution of mode 2

Let us now discuss the characteristics of mode 2, which is presented in Fig. 7 by plotting the corresponding parameters versus the inverse temperature. In general, mode 2 shifts to lower temperatures as pressure rises. The dielectric strength $\Delta\varepsilon_2(T)$ stays well below its counterpart of mode 1 for all temperatures up to 3.4 kbar, whereas upon further increasing pressure, mode 2 gains in amplitude and $\Delta\varepsilon_2(T)$ approaches the values of its counterpart $\Delta\varepsilon_1(T)$. Mode 2 significantly broadens upon cooling as indicated by a decrease of $(1 - \alpha_2)$ which, however, is shifted to lower temperatures as pressures rises. Interestingly, the temperature dependence of $\tau_2(T)$ is strongly influenced by pressure. Up to 3.1 kbar, we observe a rather steep increase which languishes upon further increasing pressure. While at 3.8 kbar, $\tau_2(T)$ increases monotonically

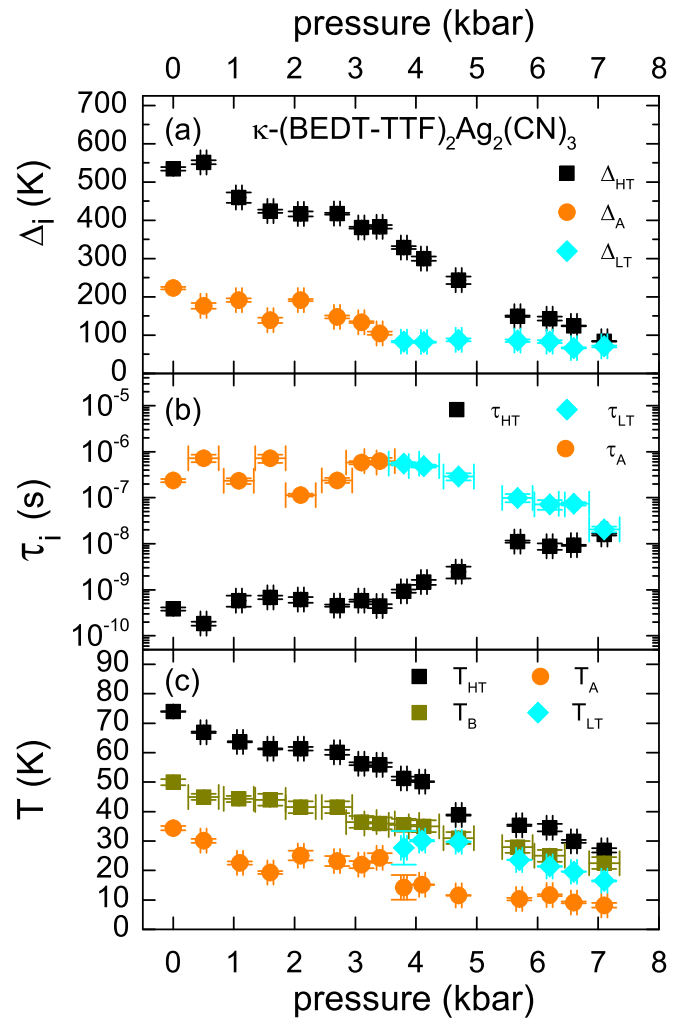


FIG. 6. (a), (b) Pressure dependence of the parameters obtained from fitting $\tau_1(T)$ of κ -(BEDT-TTF)₂Ag₂(CN)₃ with Eq. (2) [cf. Fig. 5(c)]. For $p > 3.4$ kbar, the anomaly peak is masked by the emerging LT peak such that the obtained parameters are attributed to the latter. The activation energy (a) and the timescale for the ac response in the high-temperature limit (b) of the relaxation dynamics are attributed to the HT, the anomaly and LT peaks. (c) The pressure evolution of T_{HT} , T_A , and T_{LT} together with T_B .

upon cooling, a local minimum is observed around 20 K for pressures between 4.1 and 5.7 kbar. At 6.2 kbar and above, $\tau_2(T)$ regains its strictly monotonic behavior which, however, is not as steep as before.

We conclude that the nonmonotonic temperature dependence of $\tau_2(T)$ upon applying pressure is in accordance with the findings for κ -(BEDT-TTF)₂Cu₂(CN)₃, whereas in the latter, a recovering of the purely monotonic behavior is not observed [19].

C. Pressure evolution of T_B

In the following, we verify the relation of mode 1 to the HT and LT peaks. In Fig. 8, we plot $\varepsilon_1(T)$ probed at $f = 100$ kHz and at various pressures as indicated together with the fits of the HT, LT, and A peaks from Fig. 4. The lower panels present $\tau_1(T)$ and $\tau_2(T)$ as a function of temperature

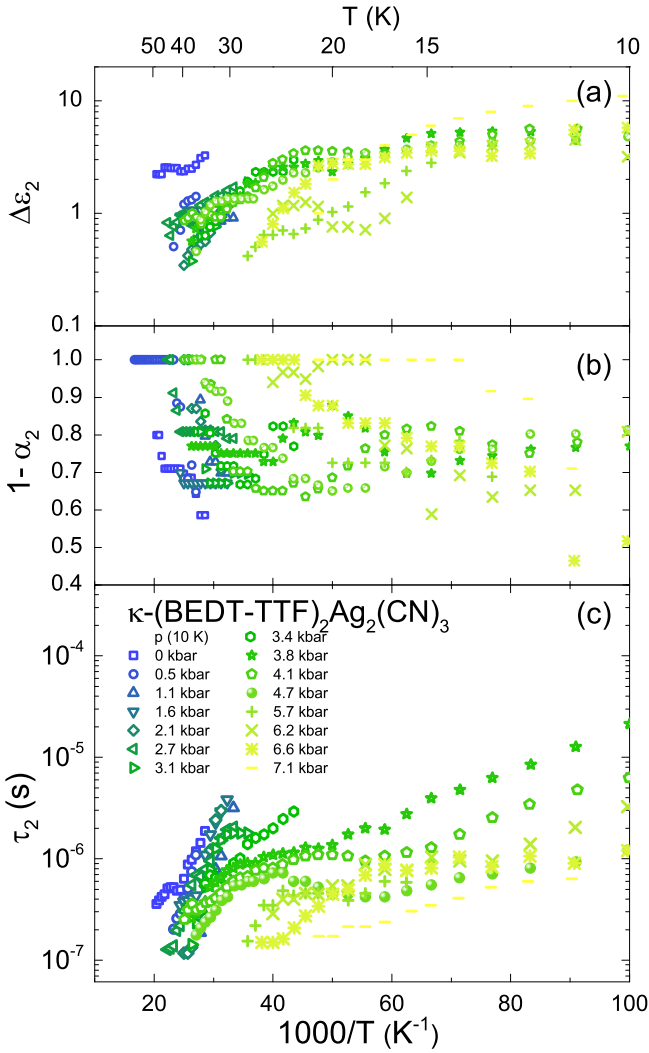


FIG. 7. Temperature dependence of the parameters describing mode 2 of κ -(BEDT-TTF)₂Ag₂(CN)₃ at various pressures as indicated. (a) Dielectric strength $\Delta\epsilon_2$ (note the logarithmic scale), (b) distribution of relaxation times $1 - \alpha_2$, and (c) mean relaxation time τ_2 in an Arrhenius plot versus inverse temperature.

including the fits of the former according to Eq. (2) for the temperature range above (black line) and below (orange and cyan line) the kink at T_B . Consistent with the procedure for κ -(BEDT-TTF)₂Cu₂(CN)₃, T_B is determined as the temperature at which the fits of $\tau_1(T)$ intersect. As expected, T_B corresponds to the kink in $\tau_1(T)$. At the same temperature, the HT peak in $\epsilon_1(T)$ diminishes and the anomaly, for pressures below 3.4 kbar, or the LT peak, for pressures above 3.4 kbar, are dominant. In particular, this confirms our assignment of the relaxation dynamics observed in $\tau_1(T)$ for $T > T_B$ to the HT peak and for $T < T_B$ to the anomaly and the LT peak in Sec. IV A. We note that $\tau_2(T)$ does not exhibit a distinct feature at $T = T_B$.

V. DISCUSSION

Our pressure-dependent investigations of the charge dynamics of κ -(BEDT-TTF)₂Ag₂(CN)₃ unveil that the di-

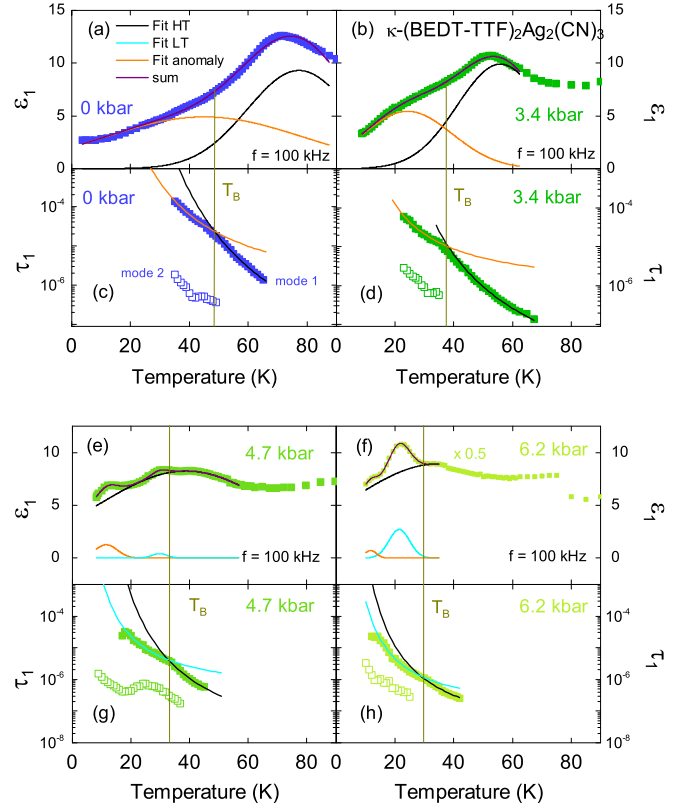


FIG. 8. Temperature dependence of the dielectric constant $\epsilon_1(T)$ of κ -(BEDT-TTF)₂Ag₂(CN)₃ probed at $f = 100$ kHz including the fits of the HT and the anomaly peak by two Gaussian modes. For pressures exceeding 3.4 kbar, a third Gaussian is used to account for the emerging LT peak. The lower panels show the relaxation times $\tau_1(T)$ and $\tau_2(T)$, the former with the fits from Figs. 5(c) and 7(c) according to Eq. (2) for the temperature range above (black line) and below (red line) the kink at T_B . This presentation emphasizes that the crossover from the HT to the LT peak coincides with the kink in $\tau_1(T)$ at T_B .

electric response contains two main dielectric contributions: the HT and the LT peak. Additionally, we find a third contribution, dubbed here anomaly (A); no corresponding response to the latter one was observed in the Cu analog κ -(BEDT-TTF)₂Cu₂(CN)₃ [19].

The HT peak was first observed as an anomalous dielectric response in κ -(BEDT-TTF)₂Cu₂(CN)₃ by Abdel-Jawad *et al.* [12]. We could show that with pressure the HT peak shifts toward lower temperatures upon approaching the IMT while its amplitude does not grow, in contrast to the LT peak. The HT peak is therefore assigned to the dielectric response within the Mott-insulating state, whereas the LT feature is attributed to a growing metallic filling fraction upon entering the coexistence regime [18–20]. Nevertheless, a full consensus on the origin of the HT peak has not been reached [16,33].

Here we could show that the HT peak in the dielectric response of κ -(BEDT-TTF)₂Ag₂(CN)₃ moves to lower temperatures when pressure increases. It is interesting to recall that also x-ray irradiation leads to a shift of the HT peak to lower temperatures [34]. High-energy irradiation causes crystal defects mainly in the anion layer and is supposed

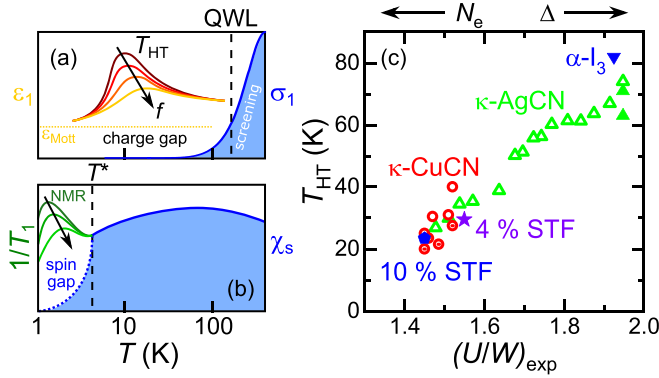


FIG. 9. (a) The relaxor-type dielectric response occurs within the Mott-insulating state, when the gap in the charge excitation spectrum has opened and, hence, screening from charge carriers breaks down. (b) Likewise, the inhomogeneous response of impurity spins, that has been observed for κ -(BEDT-TTF)₂Cu₂(CN)₃ and κ -(BEDT-TTF)₂Hg(SCN)₂Cl [41,42], is confined to the spin-gapped region below T^* [27,43]; also, for κ -(BEDT-TTF)₂Ag₂(CN)₃, such an inhomogeneous NMR relaxation has been reported at $p=0$ below 12 K [23]. (c) Position of the HT peak, T_{HT} —probed at $f=100$ kHz—plotted over the effective Coulomb repulsion U/W , as determined from optical conductivity [9], for various organic charge-transfer salts. The blue solid downward triangle indicates α -(BEDT-TTF)₂I₃ [44–46], the violet star and blue pentagon stand for κ -[(BEDT-TTF)_{1-x}(BEDT-STF)_x]₂Cu₂(CN)₃ with $x=0.04$ and 0.1 [18,20,26]. The red circles correspond to κ -(BEDT-TTF)₂Cu₂(CN)₃ measured under pressure [19], while the present results on κ -(BEDT-TTF)₂Ag₂(CN)₃ for various pressure values are included as open green triangles; solid green triangles indicate $p=0$ [15,16]. T_{HT} shifts to higher temperatures as the number of charge carriers contributing to transport, N_e , is reduced upon increasing the energy gap Δ of the insulating state.

to increase the number of charge carriers. Similar to the rising pressure, the conductivity of the sample is enhanced compared to the pristine case. This clearly indicates that the relaxor-ferroelectric HT peak is influenced by screening due to free charge carriers. Figure 9(a) illustrates how this dielectric response forms when the conductivity σ_1 has sufficiently diminished as the charge gap opens [35]. The suppression of the relaxor-type response with higher frequency goes hand in hand with the energy-dependent increase of the ac conductivity; in κ -(BEDT-TTF)₂Cu₂(CN)₃ at ambient pressure, for instance, a power-law-like ascend of $\sigma_1(\omega)$ initiates already in the kHz range at 10 K [36,37], which lines up with the reduction of $\epsilon_1(\omega)$ with increasing frequency. Generally, in the κ phase, organic Mott insulators the charge gap opens upon cooling through the QWL at T_{QWL} [9,25], resulting in a successive depletion of mobile charge carriers at temperatures below that. Indeed, the trajectory of T_{HT} is approximately parallel to T_{QWL} [38], indicating that a sufficiently opened Mott gap is required such that the relaxor-type response of the HT peak is not completely suppressed by screening.

It is informative to compare the dielectric results of the title compound with those obtained for closely related BEDT-TTF materials, such as κ -(BEDT-TTF)₂Cu₂(CN)₃—with a variation in the polymeric anions—on the one hand [18,19]

and κ -[(BEDT-TTF)_{1-x}(BEDT-STF)_x]₂Cu₂(CN)₃—with substitution at the cations—on the other hand [18,20,26]. T_{HT} rises with increasing anion mass ($m_{Ag} > m_{Cu}$) in the pristine compounds, whereas the opposite trend is observed for the BEDT-STF substitutional series. A decrease of T_{HT} upon replacing BEDT-TTF with BEDT-STF is also observed for λ -(BEDT-TTF)₂GaCl₄ and λ -(BEDT-STF)₂GaCl₄ [39,40]. This clearly evidences that mass enhancement in the anion layer has the opposite effect on the HT peak than in the donor layer, which speaks against a purely phononic origin. To also confirm this conclusion for λ -type salts, investigations on compounds with different anions, such as λ -(BEDT-TTF)₂GaBr₄ or λ -(BEDT-TTF)₂FeCl₄, are desirable.

Crucially, we should keep in mind that replacing the anions or substituting donor molecules has a significant impact on the Coulomb repulsion U and electronic correlations strength U/W . Also, the pressure evolution of T_{HT} in κ -(BEDT-TTF)₂Cu₂(CN)₃ and κ -(BEDT-TTF)₂Ag₂(CN)₃ indicates clearly that the HT peak is sensitive to U/W . The effective correlation strength can be determined experimentally from optical conductivity spectra, where the Coulomb repulsion U is given by the midinfrared Mott-Hubbard peak and the bandwidth W is determined from the width of the band. In Fig. 9(c), the temperature of the HT peak is plotted as a function of the correlation strength U/W . Besides the pressure-dependent results of the present investigations on κ -(BEDT-TTF)₂Ag₂(CN)₃ (green triangles), we include the pressure study on κ -(BEDT-TTF)₂Cu₂(CN)₃ (red circles). For comparison, data of κ -[(BEDT-TTF)_{0.96}(BEDT-STF)_{0.04}]₂Cu₂(CN)₃, κ -[(BEDT-TTF)_{0.9}(BEDT-STF)_{0.1}]₂Cu₂(CN)₃ and α -(BEDT-TTF)₂I₃ are also shown [9,18–20,26,40,44–46]. We conclude that the temperature T_{HT} linearly rises with correlation strength U/W ; as mentioned above, the reduction of T_{HT} with pressure might be caused by the enhanced screening as charge carriers are less localized when the effect of Coulomb repulsion diminishes, as sketched in Fig. 9(a).

Since the experiments on κ -(BEDT-TTF)₂Ag₂(CN)₃ map a larger phase space compared to κ -(BEDT-TTF)₂Cu₂(CN)₃, where the IMT is reached already at 1–2 kbar, we now can closely inspect the development of the dielectric features and draw general conclusions on the nature of the HT peak that were inaccessible to previous ambient pressure works [12,14,15]. The spectral weight associated with T_{HT} is negligibly small [47] compared to the Mott-Hubbard excitations in the infrared range [9,26] and can only persist as long as intrinsic charge carriers of the Mott insulator are sufficiently localized by the charge gap Δ . In addition, any relation of this dielectric feature to intrinsic Mott physics seems very unlikely since the HT peak does not move to zero when the IMT is reached [Fig. 1(c)]; instead, T_{HT} remains well defined in the region where conductivity is smallest at $T > T_{BR}$ [see Fig. 1(c)]. In contrast, the LT peak steadily increases toward the percolation limit and $T=0$, evidencing that it originates from metal-insulator phase coexistence at the first-order Mott transition [18–20]. Another distinction of the two main dielectric contributions can be seen from their frequency dependence and dielectric strength: while the polarization of the HT peak is rather weak, $\epsilon_1 \approx 10$ and T_{HT} shifts significantly with frequency, the LT feature reaches huge values

$\epsilon_1 \gg 10^2$ and the maximum temperature does not change with frequency, as it is pinned to the percolative IMT.

Based on the observed phenomenology, we suggest that the HT peak has an *extrinsic* origin, e.g., mesoscopic inhomogeneities, confining it to a poorly conducting regime deep within the Mott-insulating state. Note, a similar notion has been put forward for the spin channel, sketched in Fig. 9(b), as the NMR relaxation is dominated by an impurity response when a spin gap opens, e.g., in the compounds κ -(BEDT-TTF)₂Cu₂(CN)₃ and κ -(BEDT-TTF)₂Hg(SCN)₂Cl [27,42,43]. It remains a *desideratum* for future studies to scrutinize the LT magnetic properties of κ -(BEDT-TTF)₂Ag₂(CN)₃ to search for similar low-entropy states, possibly with a spin gap. It is intriguing to note that the reentrant behavior observed in dc transport at $T^* = 11$ K right at the IMT (Fig. 2) coincides with an extremum of the thermal expansion coefficient at 12 K [32]. In the sister compound κ -(BEDT-TTF)₂Cu₂(CN)₃, the pronounced magnetostructural anomaly at $T^* = 6$ K [48] containing an entropy of 10–20% of $R \ln 2$ [49,50] was identified as the formation of a valence bond solid by broadband electron-spin-resonance spectroscopy and various other probes [27,43].

VI. CONCLUSIONS

The frustrated Mott insulator κ -(BEDT-TTF)₂Ag₂(CN)₃ approaches the IMT when hydrostatic pressure is applied. With $p \leq 7.1$ kbar, we mostly remain on the insulating side and barely reach metallicity below 18 K; however, clear evidence for the phase coexistence regime is observed at

low temperatures. Our frequency-dependent dielectric experiments on κ -(BEDT-TTF)₂Ag₂(CN)₃ as a function of temperature, frequency, and pressure reveal that the well-known relaxor-ferroelectric response in the insulating state is not intrinsic to genuine Mott physics and most likely results from inhomogeneities. At lower temperatures it gets overwhelmed by a rapidly growing dielectric feature that is attributed to the percolative nature of the Mott transition. Thus, our previous observations of a dielectric catastrophe at the IMT in κ -(BEDT-TTF)₂Cu₂(CN)₃ [18–20] seem to be generic for the first-order transition of organic Mott insulators. It remains to be elucidated whether percolative phase coexistence may also describe the permittivity enhancement observed around the transitions of κ -(BEDT-TTF)₂Cu[N(CN)₂]Cl and κ -(BEDT-TTF)₂Hg(SCN)₂Cl [51,52]. Our endeavors demonstrate dielectric spectroscopy as a powerful method for investigations of electronic phase coexistence—in particular, when applied in pressure-dependent ac transport studies. Apart from that, we discover a reentrant insulating behavior at the IMT, similar to κ -(BEDT-TTF)₂Cu₂(CN)₃, suggesting a low-entropy spin state at temperatures below the metallic phase.

ACKNOWLEDGMENTS

We thank G. Untereiner for careful sample preparation and A. Löhle for help during the crystal growth and characterization. The project was supported by the Deutsche Forschungsgemeinschaft (DFG) via No. DR228/39-3, No. DR228/52-1, and No. DR228/68-1.

-
- [1] M. Imada, A. Fujimori, and Y. Tokura, Metal-insulator transitions, *Rev. Mod. Phys.* **70**, 1039 (1998).
 - [2] P. Hansmann, A. Toschi, G. Sangiovanni, T. Saha-Dasgupta, S. Lupi, M. Marsi, and K. Held, Mott-Hubbard transition in V₂O₃ revisited, *Phys. Status Solidi B* **250**, 1251 (2013).
 - [3] B. Keimer, S. A. Kivelson, M. R. Norman, S. Uchida, and J. Zaanen, From quantum matter to high-temperature superconductivity in copper oxides, *Nature (London)* **518**, 179 (2015).
 - [4] M. Dressel and S. Tomić, Molecular quantum materials: Electronic phases and charge dynamics in two-dimensional organic solids, *Adv. Phys.* **69**, 1 (2020).
 - [5] L. Balents, Spin liquids in frustrated magnets., *Nature (London)* **464**, 199 (2010).
 - [6] Y. Zhou, K. Kanoda, and T.-K. Ng, Quantum spin liquid states, *Rev. Mod. Phys.* **89**, 025003 (2017).
 - [7] L. Savary and L. Balents, Quantum spin liquids: A review, *Rep. Prog. Phys.* **80**, 016502 (2017).
 - [8] C. Broholm, R. J. Cava, S. A. Kivelson, D. G. Nocera, M. R. Norman, and T. Senthil, Quantum spin liquids, *Science* **367**, eaay0668 (2020).
 - [9] A. Pustogow, M. Bories, A. Löhle, R. Rösslhuber, E. Zhukova, B. Gorshunov, S. Tomić, J. A. Schlueter, R. Hübner, T. Hiramatsu, Y. Yoshida, G. Saito, R. Kato, T.-H. Lee, V. Dobrosavljević, S. Fratini, and M. Dressel, Quantum spin liquids unveil the genuine Mott state, *Nat. Mater.* **17**, 773 (2018).
 - [10] A. Georges, G. Kotliar, W. Krauth, and M. J. Rozenberg, Dynamical mean-field theory of strongly correlated fermion systems and the limit of infinite dimensions, *Rev. Mod. Phys.* **68**, 13 (1996).
 - [11] B. J. Powell and R. H. McKenzie, Quantum frustration in organic Mott insulators: From spin liquids to unconventional superconductors, *Rep. Prog. Phys.* **74**, 056501 (2011).
 - [12] M. Abdel-Jawad, I. Terasaki, T. Sasaki, N. Yoneyama, N. Kobayashi, Y. Uesu, and C. Hotta, Anomalous dielectric response in the dimer Mott insulator κ -(BEDT-TTF)₂Cu₂(CN)₃, *Phys. Rev. B* **82**, 125119 (2010).
 - [13] M. Abdel-Jawad, N. Tajima, R. Kato, and I. Terasaki, Disordered conduction in single-crystalline dimer Mott compounds, *Phys. Rev. B* **88**, 075139 (2013).
 - [14] M. Pinterić, M. Čulo, O. Milat, M. Basletić, B. Korin-Hamzić, E. Tafra, A. Hamzić, T. Ivek, T. Peterseim, K. Miyagawa, K. Kanoda, J. A. Schlueter, M. Dressel, and S. Tomić, Anisotropic charge dynamics in the quantum spin-liquid candidate κ -(BEDT-TTF)₂Cu₂(CN)₃, *Phys. Rev. B* **90**, 195139 (2014).
 - [15] M. Pinterić, P. Lazić, A. Pustogow, T. Ivek, M. Kuveždić, O. Milat, B. Gumhalter, M. Basletić, M. Čulo, B. Korin-Hamzić, A. Löhle, R. Hübner, M. Sanz Alonso, T. Hiramatsu, Y. Yoshida, G. Saito, M. Dressel, and S. Tomić, Anion effects on electronic structure and electrodynamic properties of the

- Mott insulator κ - (BEDT-TTF)₂Ag₂(CN)₃, *Phys. Rev. B* **94**, 161105(R) (2016).
- [16] M. Pinterić, D. Rivas Góngora, Ž. Rapljenović, T. Ivek, M. Čulo, B. Korin-Hamzić, O. Milat, B. Gumhalter, P. Lazić, M. Sanz Alonso, W. Li, A. Pustogow, G. Gorgen Lesseux, M. Dressel, and S. Tomić, Electrodynamics in organic dimer insulators close to Mott critical point, *Crystals* **8**, 190 (2018).
- [17] H. Fukuyama, J.-i. Kishine, and M. Ogata, Energy landscape of charge excitations in the boundary region between Dimer-Mott and charge ordered states in molecular solids, *J. Phys. Soc. Jpn.* **86**, 123706 (2017).
- [18] A. Pustogow, R. Rösslhuber, Y. Tan, E. Uykur, A. Böhme, M. Wenzel, Y. Saito, A. Löhle, R. Hübner, A. Kawamoto, J. A. Schlueter, V. Dobrosavljević, and M. Dressel, Low-temperature dielectric anomaly arising from electronic phase separation at the Mott insulator-metal transition, *npj Quantum Mater.* **6**, 9 (2021).
- [19] R. Rösslhuber, A. Pustogow, E. Uykur, A. Böhme, A. Löhle, R. Hübner, J. A. Schlueter, Y. Tan, V. Dobrosavljević, and M. Dressel, Phase coexistence at the first-order Mott transition revealed by pressure-dependent dielectric spectroscopy of κ -(BEDT-TTF)₂-Cu₂(CN)₃, *Phys. Rev. B* **103**, 125111 (2021).
- [20] Y. Saito, R. Rösslhuber, A. Löhle, M. Sanz Alonso, M. Wenzel, A. Kawamoto, A. Pustogow, and M. Dressel, Chemical tuning of molecular quantum materials κ -[(BEDT-TTF)_{1-x}(BEDT-STF)_x]₂Cu₂(CN)₃: from the Mott-insulating quantum spin liquid to metallic Fermi liquid, *J. Mater. Chem. C* **9**, 10841 (2021).
- [21] T. Komatsu, N. Matsukawa, T. Inoue, and G. Saito, Realization of superconductivity at ambient pressure by band-filling control in κ -(BEDT-TTF)₂Cu₂(CN)₃, *J. Phys. Soc. Jpn.* **65**, 1340 (1996).
- [22] Y. Kurosaki, Y. Shimizu, K. Miyagawa, K. Kanoda, and G. Saito, Mott Transition from a Spin Liquid to a Fermi Liquid in the Spin-Frustrated Organic Conductor κ -(ET)₂Cu₂(CN)₃, *Phys. Rev. Lett.* **95**, 177001 (2005).
- [23] Y. Shimizu, T. Hiramatsu, M. Maesato, A. Otsuka, H. Yamochi, A. Ono, M. Itoh, M. Yoshida, M. Takigawa, Y. Yoshida, and G. Saito, Pressure-Tuned Exchange Coupling of a Quantum Spin Liquid in the Molecular Triangular Lattice κ -(ET)₂Ag₂(CN)₃, *Phys. Rev. Lett.* **117**, 107203 (2016).
- [24] T. Itou, E. Watanabe, S. Maegawa, A. Tajima, N. Tajima, K. Kubo, R. Kato, and K. Kanoda, Slow dynamics of electrons at a metal-Mott insulator boundary in an organic system with disorder, *Sci. Adv.* **3**, e1601594 (2017).
- [25] T. Furukawa, K. Miyagawa, H. Taniguchi, R. Kato, and K. Kanoda, Quantum criticality of Mott transition in organic materials, *Nat. Phys.* **11**, 221 (2015).
- [26] A. Pustogow, Y. Saito, A. Löhle, M. Sanz Alonso, A. Kawamoto, V. Dobrosavljević, M. Dressel, and S. Fratini, Rise and fall of Landau's quasiparticles while approaching the Mott transition, *Nat. Commun.* **12**, 1571 (2021).
- [27] A. Pustogow, Thirty-year anniversary of κ -(BEDT-TTF)₂Cu₂(CN)₃: Reconciling the spin gap in a spin-liquid candidate, *Solids* **3**, 93 (2022).
- [28] C. Aebischer, D. Baeriswyl, and R. M. Noack, Dielectric Catastrophe at the Mott Transition, *Phys. Rev. Lett.* **86**, 468 (2001).
- [29] T. Hiramatsu, Y. Yoshida, G. Saito, A. Otsuka, H. Yamochi, M. Maesato, Y. Shimizu, H. Ito, Y. Nakamura, H. Kishida, M. Watanabe, and R. Kumai, Design and preparation of a quantum spin liquid candidate κ -(ET)₂Ag₂(CN)₃ having a nearby superconductivity, *Bull. Chem. Soc. Jpn.* **90**, 1073 (2017).
- [30] R. Rösslhuber, E. Uykur, and M. Dressel, Pressure cell for radio-frequency dielectric measurements at low temperatures, *Rev. Sci. Instrum.* **89**, 054708 (2018).
- [31] A. Pustogow, Y. Kawasugi, H. Sakurakoji, and N. Tajima, Chasing the spin gap through the phase diagram of a frustrated Mott insulator, [arXiv:2209.07639](https://arxiv.org/abs/2209.07639).
- [32] S. Hartmann, E. Gati, Y. Yoshida, G. Saito, and M. Lang, Thermal expansion studies on the spin-liquid-candidate system κ -(BEDT-TTF)₂Ag₂(CN)₃, *Phys. Status Solidi B* **256**, 1800640 (2019).
- [33] S. Tomić and M. Dressel, Ferroelectricity in molecular solids: a review of electrodynamic properties, *Rep. Prog. Phys.* **78**, 096501 (2015).
- [34] S. Sasaki, S. Iguchi, N. Yoneyama, and T. Sasaki, X-ray irradiation effect on the dielectric charge response in the Dimer-Mott insulator κ -(BEDT-TTF)₂Cu₂(CN)₃, *J. Phys. Soc. Jpn.* **84**, 074709 (2015).
- [35] Previous dielectric studies on κ -(BEDT-TTF)₂Cu₂(CN)₃ yield $\sigma_1 \approx 10^{-3} \Omega^{-1} \text{cm}^{-1}$ ($E \parallel c$, $f \approx 1$ MHz) associated with the frequency-dependent relaxor-type response [14]. Naturally, such a weak contribution is only seen once the dc conductivity reduces to values below that. Indeed, this happens around 30–40 K, which coincides with the temperature of the HT peak at $f \approx 1$ MHz. For $E \parallel a^*$, the contribution is two to three orders of magnitude weaker compared to in-plane measurements, but the associated $\sigma_1 \approx 10^{-6} \Omega^{-1} \text{cm}^{-1}$ ($f \approx 1$ MHz) is also crossed around T_{HT} [12,19].
- [36] M. Dressel and A. Pustogow, Electrodynamics of quantum spin liquids, *J. Phys.: Condens. Matter* **30**, 203001 (2018).
- [37] A. Pustogow, Y. Saito, E. Zhukova, B. Gorshunov, R. Kato, T.-H. Lee, S. Fratini, V. Dobrosavljević, and M. Dressel, Low-Energy Excitations in Quantum Spin Liquids Identified by Optical Spectroscopy, *Phys. Rev. Lett.* **121**, 056402 (2018).
- [38] The high-temperature feature behaves similar to the quantum Widom line: $T_{\text{HT}} \approx x T_{\text{QWL}}$ with $x = 0.3$. At that temperature, T_{HT} , the charge carrier density is reduced to approximately $N_e = N_0 \exp\{-\Delta/(k_B T_{\text{HT}})\} \approx N_0 \exp\{-T_{\text{QWL}}/T_{\text{HT}}\} \approx N_0 e^{-3} = 0.05 N_0$. In other words, conductivity is significantly reduced to a few percent compared to the QWL.
- [39] O. Iakutkina, R. Rösslhuber, A. Kawamoto, and M. Dressel, Dielectric anomaly and charge fluctuations in the non-magnetic Dimer Mott insulator λ -(BEDT-STF)₂GaCl₄, *Crystals* **11**, 1031 (2021).
- [40] R. Rösslhuber, Pressure-dependent dielectric spectroscopy measurements on organic spin liquid compounds, Ph.d. thesis, Universität Stuttgart, 2019.
- [41] Y. Shimizu, K. Miyagawa, K. Kanoda, M. Maesato, and G. Saito, Emergence of inhomogeneous moments from spin liquid in the triangular-lattice Mott insulator κ -(ET)₂Cu₂(CN)₃, *Phys. Rev. B* **73**, 140407(R) (2006).
- [42] A. Pustogow, T. Le, H.-H. Wang, Y. Luo, E. Gati, H. Schubert, M. Lang, and S. E. Brown, Impurity moments conceal low-energy relaxation of quantum spin liquids, *Phys. Rev. B* **101**, 140401(R) (2020).
- [43] B. Mijsch, A. Pustogow, M. Javaheri Rahim, A. A. Bardin, K. Kanoda, J. A. Schlueter, R. Hübner, M. Scheffler, and M. Dressel, Gapped magnetic ground state in quantum spin

- liquid candidate κ -(BEDT-TTF)₂Cu₂(CN)₃, [Science](#) **372**, 276 (2021).
- [44] M. Dressel, G. Grüner, J. P. Pouget, A. Breining, and D. Schweitzer, Field and frequency dependent transport in the two-dimensional organic conductor α -(BEDT-TTF)₂I₃, [J. Phys. I](#) **4**, 579 (1994).
- [45] T. Ivek, B. Korin-Hamzić, O. Milat, S. Tomić, C. Claus, N. Drichko, D. Schweitzer, and M. Dressel, Electrodynamic response of the charge ordering phase: Dielectric and optical studies of α -(BEDT-TTF)₂I₃, [Phys. Rev. B](#) **83**, 165128 (2011).
- [46] E. Uykur, W. Li, C. A. Kuntscher, and M. Dressel, Optical signatures of energy gap in correlated Dirac fermions, [npj Quantum Mater.](#) **4**, 19 (2019).
- [47] Generally, the plasma frequency $\omega_p = \sqrt{Ne^2/(\epsilon_0 m)}$ provides a measure of the carrier density and mass involved in a dielectric or optical process. The particle density, charge, and mass define the spectral weight $\text{SW} \propto \omega_p^2$ of its electrodynamic response. As a rough approximation, we estimate from $\Delta\epsilon \approx 10^4$ and $\tau_0^{-1} \approx 10^5$ Hz [14] the plasma frequency of the relaxor dielectric response as $\omega_p \approx \tau_0 \sqrt{\Delta\epsilon} \approx 3 \times 10^{-4} \text{ cm}^{-1}$, which is more than seven to eight orders of magnitude smaller than optical Mott-Hubbard excitations of one electron per formula unit in κ -(BEDT-TTF)₂Cu₂(CN)₃, yielding $\omega_p \approx 10^4 \text{ cm}^{-1}$ [9,26]. In another approach, we integrate the spectral weight of the relaxor response up to $\omega_0 \approx U/\hbar c \approx 2000 \text{ cm}^{-1}$, which gives $\omega_p \approx 1 \text{ cm}^{-1}$. The two results correspond to carrier densities $N_{\text{diel}}/N_{\text{opt}} \approx 10^{-15}$ and 10^{-8} , respectively, which provide clear evidence that the relaxor-type dielectric response is no intrinsic feature of intradimer excitations of correlated electrons. Instead, the experimental observations fit well with polarization properties on larger length scales with small N related to disorder and inhomogeneities.
- [48] R. S. Manna, M. de Souza, A. Brühl, J. A. Schlueter, and M. Lang, Lattice Effects and Entropy Release at the Low-Temperature Phase Transition in the Spin-Liquid Candidate κ -(BEDT-TTF)₂Cu₂(CN)₃, [Phys. Rev. Lett.](#) **104**, 016403 (2010).
- [49] S. Yamashita, Y. Nakazawa, M. Oguni, Y. Oshima, H. Nojiri, Y. Shimizu, K. Miyagawa and K. Kanoda, Thermodynamic properties of a spin-1/2 spin-liquid state in a κ -type organic salt, [Nat. Phys.](#) **4**, 459 (2008).
- [50] E. Yesil, S. Imajo, S. Yamashita, H. Akutsu, Y. Saito, A. Pustogow, A. Kawamoto, and Y. Nakazawa, Thermodynamic Properties of the Mott Insulator-Metal Transition in a Triangular Lattice System Without Magnetic Order, [Phys. Rev. B](#) **107**, 045133 (2023).
- [51] P. Lunkenheimer, J. Müller, S. Krohns, F. Schrettle, A. Loidl, B. Hartmann, R. Rommel, M. de Souza, C. Hotta, J. A. Schlueter, and M. Lang, Multiferroicity in an organic charge-transfer salt that is suggestive of electric-dipole-driven magnetism, [Nat. Mater.](#) **11**, 755 (2012).
- [52] E. Gati, J. K. H. Fischer, P. Lunkenheimer, D. Zielke, S. Köhler, F. Kolb, H. A. K. von Nidda, S. M. Winter, H. Schubert, J. A. Schlueter, H. O. Jeschke, R. Valentí, and M. Lang, Evidence for Electronically Driven Ferroelectricity in a Strongly Correlated Dimerized BEDT-TTF Molecular Conductor, [Phys. Rev. Lett.](#) **120**, 247601 (2018).